

Acoustic superlens using membrane-based metamaterials

Jong Jin Park, Choon Mahn Park, K. J. B. Lee, and Sam H. Lee

Citation: [Applied Physics Letters](#) **106**, 051901 (2015); doi: 10.1063/1.4907634

View online: <http://dx.doi.org/10.1063/1.4907634>

View Table of Contents: <http://scitation.aip.org/content/aip/journal/apl/106/5?ver=pdfcov>

Published by the [AIP Publishing](#)

Articles you may be interested in

[A lightweight low-frequency sound insulation membrane-type acoustic metamaterial](#)

AIP Advances **6**, 025116 (2016); 10.1063/1.4942513

[Acoustic superlens using Helmholtz-resonator-based metamaterials](#)

Appl. Phys. Lett. **107**, 193505 (2015); 10.1063/1.4935589

[Acoustic planar hyperlens based on anisotropic density-near-zero metamaterials](#)


Appl. Phys. Lett. **107**, 133503 (2015); 10.1063/1.4932097

[Active control of membrane-type acoustic metamaterial by electric field](#)





Appl. Phys. Lett. **106**, 091904 (2015); 10.1063/1.4913999

[Analytical coupled vibroacoustic modeling of membrane-type acoustic metamaterials: Membrane model](#)

J. Acoust. Soc. Am. **136**, 969 (2014); 10.1121/1.4892870



Instruments for Advanced Science

 <p>Gas Analysis</p> <ul style="list-style-type: none">dynamic measurement of reaction gas streamscatalysis and thermal analysismolecular beam studiesdissolved species probesfermentation, environmental and ecological studies	 <p>Surface Science</p> <ul style="list-style-type: none">UHV TPDSIMSend point detection in ion beam etchelemental imaging - surface mapping	 <p>Plasma Diagnostics</p> <ul style="list-style-type: none">plasma source characterizationetch and deposition process reactionkinetic studiesanalysis of neutral and radical species	 <p>Vacuum Analysis</p> <ul style="list-style-type: none">partial pressure measurement and control of process gasesreactive sputter process controlvacuum diagnosticsvacuum coating process monitoring
--	---	---	---

Contact Hiden Analytical for further details:
www.HidenAnalytical.com
info@hiden.co.uk
[CLICK TO VIEW](#) our product catalogue

Acoustic superlens using membrane-based metamaterials

Jong Jin Park,¹ Choon Mahn Park,¹ K. J. B. Lee,^{2,a)} and Sam H. Lee^{1,b)}

¹*Institute of Physics and Applied Physics, Yonsei University, Seoul 120-749, South Korea*

²*Department of Physics, Ewha Womans University, Seoul 120-750, South Korea*

(Received 17 September 2014; accepted 26 January 2015; published online 2 February 2015)

We report construction of an acoustic superlensing using two dimensional membrane-based negative-density metamaterials. When two point sources separated by a distance of $1/17$ of the wavelength are placed near to a surface of the metamaterial slab, well-resolved images are formed on the opposite surface across the slab. The mechanism for the subwavelength resolution is the surface wave stemming from negative density. Potential applications include acoustic imaging and sensing. © 2015 AIP Publishing LLC. [<http://dx.doi.org/10.1063/1.4907634>]

Electromagnetic or acoustic waves emitted from a source include evanescent waves conveying the subwavelength information. Decaying evanescent waves are responsible for the diffraction limit and hence, focusing waves into spot sizes smaller than one third of the wavelength (λ) is not possible using conventional methods. Overcoming the diffraction limit has been an important issue for high resolution imaging. The most fascinating idea is probably that a medium of negative index of refraction, not naturally existing, can strongly amplify the near-field evanescent waves and so perfectly focus all the information of the source.¹ Since then, the superlens concept has been evolved and several experimental demonstrations have been reported by using various electromagnetic metamaterials with negative index of refraction, negative permittivity, or negative permeability at optical, microwave, or infrared frequencies.^{2–12}

The theoretical and experimental success of the electromagnetic metamaterials has led to analogous acoustic metamaterials and the realization of acoustic metamaterials with negative density and/or negative modulus has been demonstrated.^{13–18} As an approach to the development of an acoustic superlens, ultrasound-focus of $\lambda/2$ was experimentally demonstrated by using an array of Helmholtz resonators filled with water, which mapped to negative mass density and negative compressibility by transmission line model.¹⁹ A flat lens of a phononic crystal exhibiting negative refraction, albeit in Bragg scattering scheme, was reported to be able to focus up to 0.37λ .²⁰ Recently, a 3D holey-structured metamaterial was reported to achieve acoustic imaging down to a feature size of $\lambda/50$ as a result of Fabry-Pérot resonances.²¹ Here, we present a realization of acoustic imaging with $\lambda/17$ resolution by first using a membrane-based negative-density metamaterial which can highly localize surface waves and so amplify the evanescent waves.

Even though first proposed superlensing was using double negative materials,¹ single negative electromagnetic metamaterial slabs also have been used to construct successful superlenses.^{2–6,10,12} Also, acoustic single negative metamaterials with negative density (ρ -NG metamaterial) were theoretically and numerically demonstrated to be capable of

making superlensing.²² In Ref. 22, it was shown that a point source placed at a close distance from the surface of the ρ -NG metamaterial slab excites a surface vibration pattern on the surface, which generates evanescent waves in the bulk of the ρ -NG metamaterial. In case the thickness of the slab is not too thick, another surface vibration pattern of the same shape is excited by the tail of the evanescent wave on the other surface across the slab. This vibration pattern produces the image with subwavelength resolution. Although the ρ -NG metamaterial can highly localize surface waves over a wide range of the evanescent wave vectors, dimension of a unit cell and structural dissipation lead to practical limitations on resolution beyond the diffraction limit. The structural dissipation could be controlled in the membrane-based two-dimensional ρ -NG metamaterial to a remarkably small level by our group.²³ In this work, we report a demonstration of acoustic superlensing by fabricating membrane-based two-dimensional ρ -NG metamaterial with a lattice constant as small as $\lambda/17$. Our superlens sharply resolves two sound waves separated by a distance of the lattice constant.

Fabricating the negative-density metamaterial using membrane needs very careful treatment. Our design for membrane-covered unit came from an embroidery hoop which consists of two rings with slightly different diameters. We prepared three kinds of units made of plastics: (i) $25\text{ mm} \times 25\text{ mm}$ square of thickness 1.5 mm with a shallow cylindrical opening of diameter 18 mm and height 2.6 mm in the center, (ii) an outer ring of diameter 18 mm and thickness 1.3 mm, and (iii) a joint which can connect four squares as shown in the small box at the right bottom of Fig. 1(a). Each opening was covered tightly by low-density polyethylene film of thickness 0.01 mm using the ring. The membrane-covered square units were left saturated in the sense that the resonant frequency was stabilized in the environment, while monitoring the changes of the resonant frequencies. The resonant frequency of each unit was fine-tuned with tiny mass to have the same value. Two-dimensional slab of size $84\text{ mm} \times 480\text{ mm}$ as shown in Fig. 1(a) was assembled by 116 membrane-covered units which have the resonance frequency, $f_m = 690 \pm 2\text{ Hz}$.

The assembled structure exhibits a negative effective density at frequencies below a certain cutoff frequency (ω_c) such as^{22,23}

^{a)}Electronic mail: kjblee@ewha.ac.kr

^{b)}Electronic mail: samlee@yonsei.ac.kr

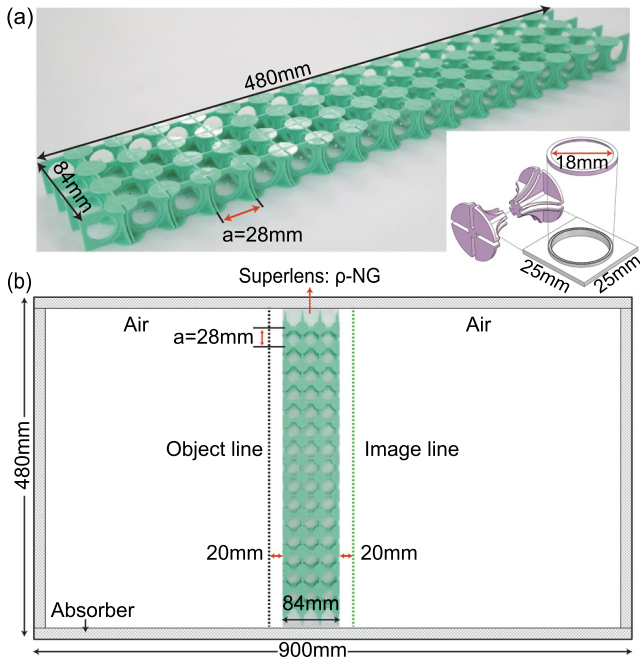


FIG. 1. Superlensing slab made of membrane-based acoustic metamaterial. (a) Metamaterial slab is consisting of 116 plastic squares, each with a circular window. The circular openings are covered with thin membranes and the assembled metamaterial has a lattice constant, $a = 28$ mm. (b) The negative-density superlens is sandwiched in between two rigid plastic plates of dimensions $900 \text{ mm} \times 480 \text{ mm} \times 5 \text{ mm}$ the edge of which is closed by anechoic walls. The object and the image lines are located 20 mm from the left and the right interfaces between the air and the metamaterial, respectively.

$$\rho_{eff}(\omega) = \rho' \left(1 - \frac{\omega_c^2}{\omega^2} \right), \quad (1)$$

where ρ' is the averaged mass density of the air and membrane. The effective modulus is equivalent to the air modulus in this system.²³ On the other hand, the wave vector (k_y) of the surface waves at the interface between the air and the metamaterial can be explicitly expressed as

$$k_y(\omega) = k_0 \sqrt{\frac{\rho_{eff}(\omega)}{\rho_0 + \rho_{eff}(\omega)}}, \quad (2)$$

where k_0 and ρ_0 are the wave vector in the air and the density of air, respectively. It is clear that the wave vector of the surface wave reaches asymptotically infinity when $\rho_{eff} \rightarrow -\rho_0$. It occurs at the frequency, $\omega = \omega_c / \sqrt{2}$ if assuming that $\rho' \approx \rho_0$. The cutoff frequency can be roughly estimated from the resonance frequency f_m of the membrane-covered square unit by following the theoretical analysis¹⁶ which yields an approximate relation, $\omega_c \approx \sqrt{M_m / (\rho' V)} \omega_m$. M_m is the effective mass determining the resonance frequency ω_m , V is the effective volume of the unit cell of the metamaterial, and $\omega_m = 2\pi f_m$. With the approximation, $\rho' \approx \rho_0$ again, the proportional coefficient between two frequencies ω_c and ω_m can be obtained by the ratio of the effective length (l_m) of the air column moving together with the membrane in a single square unit to the lattice constant of the metamaterial, i.e., $\sqrt{l_m / a}$. Hence using that $l_m \sim 55.3$ mm from the experimental setup for the measurements of ω_m , $a = 28$ mm, and $f_m = 690$ Hz, the cutoff frequency is roughly estimated as

$f_c \sim 970$ Hz, suggesting the diverging wave vector of the surface waves at the frequency near 686 Hz. This crude estimation turns out to be only 4% off from the experimentally observed value of 714 Hz below.

For experimental measurements, two plastic plates of size $900 \times 480 \text{ mm}^2$ and thickness 5 mm were placed on the top and the bottom of the metamaterial and the edge-gap between the plates was closed with an absorber. The object and the image lines were prepared at 20 mm apart from the left and the right interfaces between air and the ρ -NG metamaterial, respectively, as shown in Fig. 1(b).

To demonstrate that sound waves emitted from a point source really do focus in subwavelength by enhancing the evanescent waves through the ρ -NG metamaterial we fabricated, a single speaker of diameter 20 mm was placed at the middle of the object line and the pressures on and up to 30 mm beyond the image line were measured by scanning a microphone. The radiation pattern of the small loudspeaker is circular and the radiation pressure rapidly decreases with the distance when there is no metamaterial slab. On the other hand, when ρ -NG metamaterial slab is placed in front of the speaker, a surface vibration pattern is excited on the metamaterial surface across the slab, and it generates the image of the small loudspeaker, making the pressure intensity at the focus much bigger than that at the same place without the metamaterial slab. We found that the incident sound waves of a frequency 714 Hz made a sharp image on the image line. Fig. 2(a) shows the pressure-intensity profile of the sound waves after passing through the ρ -NG metamaterial slab. In Fig. 2(b), pressure distribution data on the image line, with and without the metamaterial slab, are shown in red and blue dots, respectively. Notably, the width of the peak is narrowed by a factor of 10 from about $\lambda/2$ without the slab to $\lambda/22$ by inserting the slab. To clearly compare the widths of the peaks, the intensities are normalized to have the same height, but the peak intensity with the metamaterial is 17 times higher than that of the case without it. This remarkable energy concentration is due to excitation of surface waves of many different wavelengths which add up to make the sharp peak. Since acoustic wave equation for air is valid in the space beyond the metamaterial slab, this concentrated intensity in the image line is expected to radiate as if it is a point source. This intensity on the image line was about 78% of that of the incident sound just before entering the slab. Therefore, the metamaterial slab provided an effective channel for sound transmission in this special fashion.

To observe a subwavelength resolution of two point sources using our structure, two identical speakers separated by a distance of lattice constant 28 mm or $\lambda/17$ were placed at the object line. For the purpose of the best resolution, the speakers were activated to generate out-of-phase sounds of frequency 714 Hz to each other so that the two incident waves were clearly distinguished. The radiation pattern of two speakers is just like two circular waves interfered in out-of-phase when there is no ρ -NG metamaterial slab. The pressure-intensity profile after passing through the ρ -NG metamaterial slab, as shown in Fig. 3(a), demonstrates that two images are definitely separated as much as two sources. The pressure-intensity on the image line denoted by red dots in Fig. 3(b) confirms again that sound waves emitted from two point sources separated by $\lambda/17$ indeed form ultra-fine

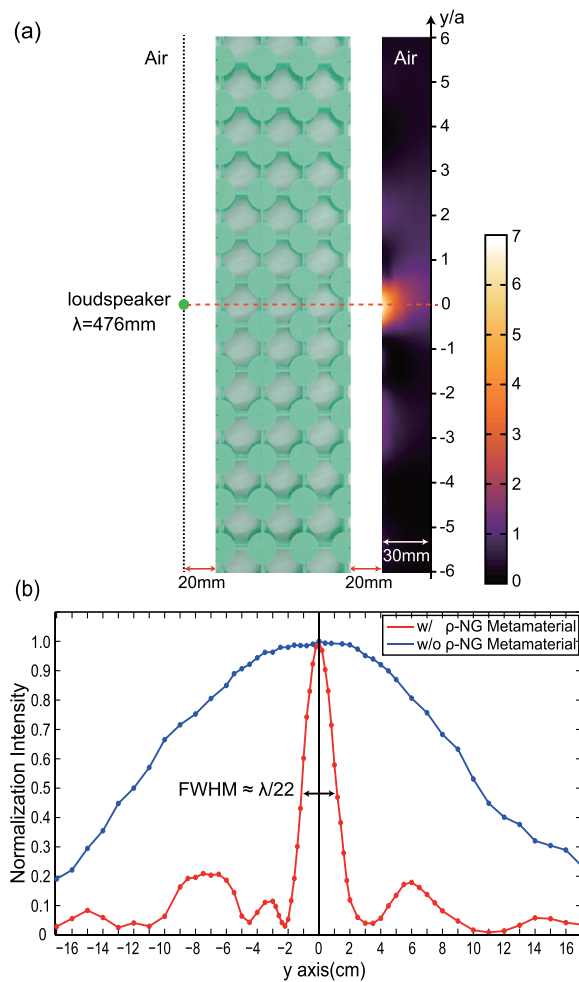


FIG. 2. Experimental result with one point source of 714 Hz. (a) Pressure-intensity profile of the sound waves after passing through the ρ -NG metamaterial slab. (b) Normalized pressure-intensity data on the image line. The red (blue) dots indicate the data in the presence (absence) of the ρ -NG metamaterial. The incident sounds are focused as thin as 22 mm or $\lambda/22$.

images overcoming the diffraction limit through our ρ -NG metamaterial slab. In other words, images of two acoustic objects separated by a distance as close as the lattice constant of the ρ -NG metamaterial slab are clearly resolved. The FWHM's for two images is as sharp as 18 mm or $\lambda/26$ and 20 mm or $\lambda/24$, respectively. The peak intensities through the slab were amplified about 93-fold and 47-fold, respectively, compared to those without the ρ -NG metamaterial slab. These extremely high enhancements of intensities are simply due to the out-of-phase sources.

We repeated the experiments with two in-phase point sources separated by a distance of 56 mm or $\lambda/8.5$, which is twice the lattice constant. The radiation pattern of two speakers is just like two circular waves interfered in in-phase when there is no ρ -NG metamaterial slab. By locating two sources in two unit-cells away from each other, two in-phase source signals are prepared to be distinguished. The pressure-intensity profile of two in-phase sound sources of the frequency 714 Hz after passing through our ρ -NG metamaterial, as expected from the above observation, exhibits the ultra-high resolution as shown in Fig. 4(a). The normalized pressure-intensities on the image line are plotted in Fig. 4(b). A remarkable resolution of two images (red dots) was

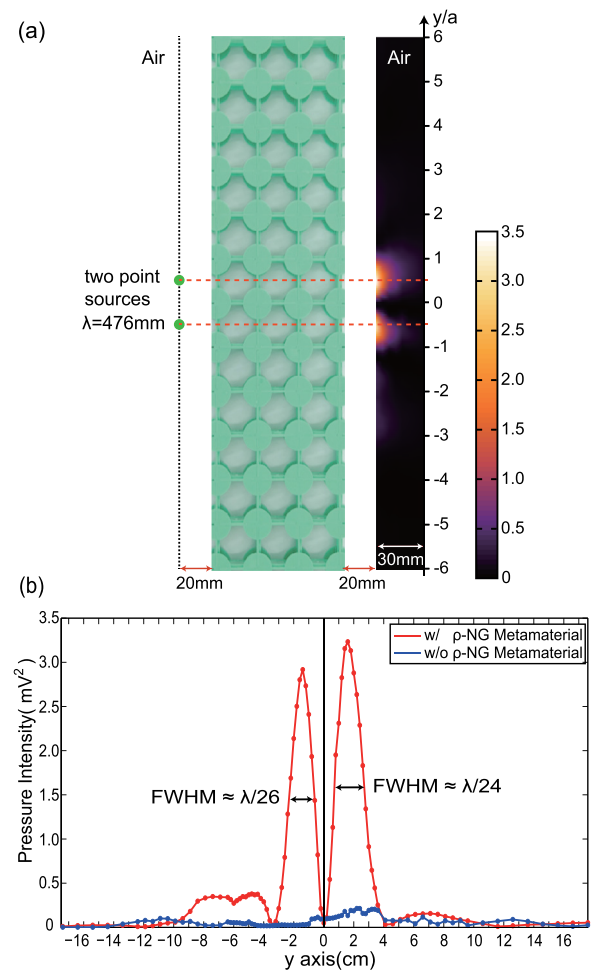


FIG. 3. Experimental result with two out-of-phase acoustic point sources separated by a distance of a lattice constant, $\lambda/17$. Two identical speakers are activated at the frequency 714 Hz with out-of-phase to each other. (a) Pressure-intensity profile of the two sound waves after passing through the ρ -NG metamaterial slab. (b) Pressure-intensity data on the image line. The red (blue) dots indicate the data in the presence (absence) of the ρ -NG metamaterial. The two sound sources separated by $\lambda/17$ are clearly resolved.

observed with the metamaterial slab compared to the wide distribution (blue dots) without the metamaterial slab. The peak intensities of two images with the slab are about 2.9-fold and 3.3-fold enhanced if compared to those without the slab, respectively. The two sounds are focused roughly as thin as 19 mm or $\lambda/25$ and 23 mm or $\lambda/21$, respectively. Unexpected side lobes are observed as can be seen in Figures 2(b), 3(b), and 4(b) on the right and left side of the main peaks. One may consider the possibility that these patterns reflect diffraction from the periodicity of the lattice. However, the characteristic inter-peak distance of ~ 7 cm is far shorter than the wavelength, $\lambda = 47.6$ cm. Another possibility is that these are mere artifacts stemming from uniformity-error in the metamaterial. We constructed 116 membrane-covered unit cells with the average resonance frequency of 690 Hz, but the resonance frequencies have deviation from cell to cell, with the distribution 690 ± 2 Hz. Since the dispersion curve is very sensitive to the resonant frequency, this amount of error in homogeneity and symmetry of the metamaterial system resulted in the artificial signals along the surface of the metamaterial. However, sharp central peak stands clearly over these aberrations.

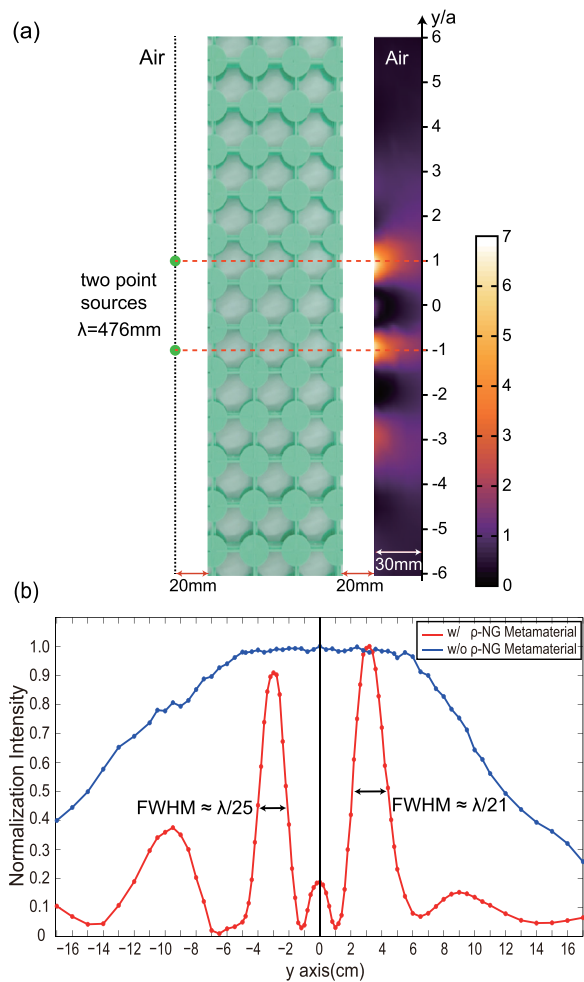


FIG. 4. Experimental result with two in-phase point sources separated by a distance of twice the lattice constant, $\lambda/8.5$. Two identical speakers are activated at the frequency of 714 Hz. (a) Pressure-intensity profile of the two sound waves after passing through the ρ -NG metamaterial slab. (b) Normalized pressure-intensity data on the image line. The red (blue) dots indicate the data in the presence (absence) of the ρ -NG metamaterial.

In this letter, we demonstrated an experimental realization of an acoustic superlens first using two-dimensional membrane-based negative-density metamaterial slab. Our superlensing system resulted in a remarkably high resolution of two point sources separated by $\lambda/17$. The resolution of $\lambda/17$ far exceeds the smallest resolution allowed by the diffraction limit. The evanescent waves incident on our low-dissipative ρ -NG metamaterial slab were amplified significantly and about 78% of the incident waves was refocused on the image line. The refocusing peak-intensity was 17-fold enhanced if compared with that in the absence of the superlensing system. In this sense, our superlensing system turns out to be quite effective even compared to the previous systems using various electromagnetic metamaterials.^{3,5,10}

Artificial structures engineered on a sub-wavelength level, metamaterials, have produced exotic characteristics of wave propagation. A wide range of single and double negative constitutive parameters in both electromagnetics and acoustics has made unbelievable phenomena such as cloaking²⁴ and superlensing possible in reality. In practical fabrications of these devices, dissipation control is one of the main difficulties. The membrane-based metamaterials, in this matter, are remarkably efficient since the membranes move together with the fluid yielding a small friction. Our membrane-based negative-density metamaterial may be of a big help toward developing a practical acoustic superlens, hyperlens, perfect lens, and cloak.

This work was supported by the National Research Foundation of Korea (NRF) grant funded by the Korea government (MSIP) (Grant No. 2008-0061893).

- ¹J. B. Pendry, *Phys. Rev. Lett.* **85**, 3966 (2000).
- ²Z. Liu, N. Fang, T.-J. Yen, and X. Zhang, *Appl. Phys. Lett.* **83**, 5184 (2003).
- ³N. Fang, Z. Liu, T.-J. Yen, and X. Zhang, *Opt. Express* **11**, 682 (2003).
- ⁴N. Fang, H. Lee, C. Sun, and X. Zhang, *Science* **308**, 534 (2005).
- ⁵H. Lee, Y. Xiong, N. Fang, W. Srituravanich, S. Durant, M. Ambati, C. Sun, and X. Zhang, *New J. Phys.* **7**, 255 (2005).
- ⁶D. Melville and R. Blaikie, *Opt. Express* **13**, 2127 (2005).
- ⁷A. A. Houck, J. B. Brock, and I. L. Chuang, *Phys. Rev. Lett.* **90**, 137401 (2003).
- ⁸A. Grbic and G. V. Eleftheriades, *Phys. Rev. Lett.* **92**, 117403 (2004).
- ⁹A. N. Lagarkov and V. N. Kissel, *Phys. Rev. Lett.* **92**, 077401 (2004).
- ¹⁰T. Taubner, D. Korobkin, Y. Urzhumov, G. Shvets, and R. Hillenbrand, *Science* **313**, 1595 (2006).
- ¹¹B.-I. Popa and S. A. Cummer, *Phys. Rev. E* **73**, 016617 (2006).
- ¹²G. Lipworth, J. Ensworth, K. Seetharam, D. Huang, J. S. Lee, P. Schmalenberg, T. Nomura, M. S. Reynolds, D. R. Smith, and Y. Urzhumov, *Sci. Rep.* **4**, 3642 (2014).
- ¹³Z. Liu, X. Zhang, Y. Mao, Y. Y. Zhu, Z. Yang, C. T. Chan, and P. Sheng, *Science* **289**, 1734 (2000).
- ¹⁴J. Li and C. T. Chan, *Phys. Rev. E* **70**, 055602 (2004).
- ¹⁵N. Fang, D. Xi, J. Xu, M. Ambati, W. Srituravanich, C. Sun, and X. Zhang, *Nat. Mater.* **5**, 452 (2006).
- ¹⁶S. H. Lee, C. M. Park, Y. M. Seo, Z. G. Wang, and C. K. Kim, *Phys. Lett. A* **373**, 4464 (2009).
- ¹⁷S. H. Lee, C. M. Park, Y. M. Seo, Z. G. Wang, and C. K. Kim, *J. Phys.: Condens. Matter* **21**, 175704 (2009).
- ¹⁸S. H. Lee, C. M. Park, Y. M. Seo, Z. G. Wang, and C. K. Kim, *Phys. Rev. Lett.* **104**, 054301 (2010).
- ¹⁹S. Zhang, L. Yin, and N. Fang, *Phys. Rev. Lett.* **102**, 194301 (2009).
- ²⁰A. Sukhovich, B. Merheb, K. Muralidharan, J. O. Vasseur, Y. Pennec, P. A. Deymier, and J. H. Page, *Phys. Rev. Lett.* **102**, 154301 (2009).
- ²¹J. Zhu, J. Christensen, J. Jung, L. Martin-Moreno, X. Yin, L. Fok, X. Zhang, and F. J. Garcia-Vidal, *Nat. Phys.* **7**, 52 (2011).
- ²²M. Ambati, N. Fang, C. Sun, and X. Zhang, *Phys. Rev. B* **75**, 195447 (2007).
- ²³C. M. Park, J. J. Park, S. H. Lee, Y. M. Seo, C. K. Kim, and S. H. Lee, *Phys. Rev. Lett.* **107**, 194301 (2011).
- ²⁴D. Schurig, J. J. Mock, B. J. Justice, S. A. Cummer, J. B. Pendry, A. F. Starr, and D. R. Smith, *Science* **314**, 977 (2006).